

RESEARCH ARTICLE

10.1029/2023JD038829

Key Points:

- The leading intermodel spread in winter surface air temperature change at the end of the 21st century over the Eurasian continent is a warming pattern from the CMIP6 models
- The large-circulation changes in the sea-level pressure, the tilting trough, and jets are highly associated with this intermodel spread
- All these changes might be traced to the warm SST changes in the western North Pacific and the tropical Atlantic

Correspondence to:

D. Huang and A. Huang,
huangdq@nju.edu.cn;
anhuang@nju.edu.cn

Citation:

Liu, A., Huang, D., & Huang, A. (2023). The leading intermodel spread of the projected changes in the Eurasian continent winter surface air temperature and large-scale circulations from the CMIP6 simulations. *Journal of Geophysical Research: Atmospheres*, 128, e2023JD038829. <https://doi.org/10.1029/2023JD038829>



Received 10 MAR 2023

Accepted 29 APR 2023

Author Contributions:

Conceptualization: Danqing Huang
Funding acquisition: Danqing Huang
Methodology: Anqi Liu, Danqing Huang
Software: Anqi Liu
Supervision: Danqing Huang
Validation: Danqing Huang
Writing – original draft: Anqi Liu
Writing – review & editing: Danqing Huang, Anning Huang

The Leading Intermodel Spread of the Projected Changes in the Eurasian Continent Winter Surface Air Temperature and Large-Scale Circulations From the CMIP6 Simulations

Anqi Liu¹, Danqing Huang¹ , and Anning Huang¹ ¹School of Atmospheric Sciences, Nanjing University, Nanjing, China

Abstract This study investigates the intermodel spread of changes in the Eurasian winter surface air temperature (SAT) based on Coupled Model Intercomparison Project 6 (CMIP6) and explains it from the perspective of circulation under shared socioeconomic pathway 2–4.5. Results show that the leading intermodel spread of Eurasian SAT change, derived from the intermodel empirical orthogonal function analysis (EOF), is characterized by a warming pattern of SAT change. This warming pattern is associated with the changes in the weakened Siberian High and Aleutian Low, the weakened subtropical jet, the poleward polar jet, and the tilting trough. The combination of these circulations has prevented the intrusion of the cold air to the south and therefore results in the warming SAT change pattern. Their relative contribution weights of the weakened Siberian High and Aleutian Low, the tilting East Asian trough, the weakened subtropical jet, and the poleward polar jet are 12.73%, 20.43%, 30.24%, 20.96%, and 15.64%, respectively. All these changes may be traced to the warm sea surface temperature (SST) changes in the western North Pacific and tropical Atlantic Ocean, via the meridional temperature gradient and wave trains, respectively. These warmings would be the potential metrics for reducing the intermodel uncertainties of the winter SAT projection at the end of the 21st century over the Eurasian continent.

Plain Language Summary There are still large intermodel uncertainties in the projection of the winter SAT over the Eurasian continent. In this study, the intermodel EOF is utilized to derive the intermodel spread in the winter SAT change at the end of the 21st century over the Eurasian continent. The leading mode is a warming pattern over Eurasia, which is closely related to the large-scale circulations, including the changes in the weakened Siberian High and Aleutian Low, the tilt of the East Asian trough, the weakened western subtropical jet, and the northward shift of the eastern polar front jet. All these changes may be traced to the warming in the western North Pacific and the tropical Atlantic. Our findings provide a perspective to improve the projection of Eurasian winter SAT.

1. Introduction

Recently, although the global average surface temperature has enhanced (Rama et al., 2022; Solomon et al., 2007), Eurasian midlatitudes have experienced cold winters unexpectedly (Cohen et al., 2014; Honda et al., 2009), which has attracted a lot of attention. One of the most crucial climate indicators (Han & Sun, 2018), the surface air temperature (SAT) over the Eurasian continent in the winter has a significant impact on the economy and society (Luo & Wang, 2017). The two leading modes of Eurasian SAT anomalies have been extracted (Mori et al., 2014), the uniform warming over Eurasian and the warm Arctic-cold Eurasia pattern, which is traced to the Arctic oscillation and the sea-ice decline, respectively (Chen & Luo, 2019; Inoue et al., 2012; Luo et al., 2016; Mori et al., 2014; Overland et al., 2011). Both the variability of the atmospheric circulation (D. Luo et al., 2016; D. H. Luo et al., 2016; McCusker et al., 2016; Yao et al., 2016) and the high latitudes thermal conditions (Cohen et al., 2012; Han & Sun, 2018; Mori et al., 2014) have impacts on the variations in the Eurasian SAT in winter. It is important to understand the model uncertainties in Eurasian SAT in winter, particularly for the projection of future regional climate.

Previous studies suggested that cold winters over Eurasia correspond to an intensified Aleutian low and Siberian high at the surface (Takaya & Nakamura, 2005a, 2005b; Zhang et al., 1997), a deepened East Asian trough (Leung & Zhou, 2015) and the long-lived Ural Blocking (D. Luo et al., 2016, 2019, 2021; Yao et al., 2017) at the middle level, and the strong jet streams at the upper level (Luo & Zhang, 2015). Furthermore, both the southwestward displacement and the tilting East Asian trough would contribute to the cold anomalies over Southeast Asia, by

controlling the northerlies (Leung & Zhou, 2015; Lu et al., 2016; Wang et al., 2009; Zhang et al., 2015). In winter, the activities of two branches of the jet streams over Eurasia, the subtropical jet at $\sim 25^{\circ}\text{N}$ and the polar front jet at $\sim 55^{\circ}\text{N}$ (Chowdary et al., 2019; Nakamura et al., 2010), such as enhanced subtropical jet and the concurrent variation in location and intensity of the two jets, are linked to the Eurasian SAT change (Ha et al., 2012; Huang et al., 2019; Liao & Zhang, 2013; Luo & Zhang, 2015; Yang et al., 2002; Zhang et al., 2008, 2019; Zhang & Xiao, 2013). Therefore, it is complex and meaningful to explore the change in Eurasian SAT and its relationship with the changes in the large-scale circulation systems.

Some studies have dug into the projection of the SAT by the climate models (Fan et al., 2020; Moss et al., 2010). The Coupled Model Intercomparison Project (CMIP) has improved from CMIP5 to CMIP6 for capturing the features of climatological temperature and related circulation systems (Jiang et al., 2020; Xu et al., 2016), with promoted horizontal resolutions, physical processes parameterizations, and the addition of processes and components in the Earth system (Eyring et al., 2019; Wu et al., 2022). Furthermore, CMIP6 is equipped with more kinds of models under new shared socioeconomic pathway (SSP) scenarios than before (Eyring et al., 2016). However, simulations are still challenging because of the large uncertainty (Aru et al., 2021; Monerie et al., 2020; Yao et al., 2016), exhibiting a large spread across models in historical experiments and future projections in simulating both SAT and precipitation (Fan et al., 2020; Huang et al., 2022; Xu & Fan, 2022) suffered from large-scale circulation (Gong et al., 2014; Zhou et al., 2020).

Our recent studies have physically linked the intermodel spread of simulated East Asian summer monsoon rainfall (Huang et al., 2022) and Eurasian winter SAT (Liu et al., 2022) with the circulation variations in the historical experiments in CMIP6, simulating the climate change observed from 1850 to 2014, proving that assessing the intermodel uncertainty problem from the perspective of the physical relationship with the circulation is desirable (Wang et al., 2021). Here, we investigated whether the intermodel spread of Eurasian SAT and its relation with the main circulations found in historical experiments would persist into the warmer future or not. Understanding this will help us to constrain the SAT and enhances the credibility of the projections in future study. Thus, it is critical to investigate the intermodel spread of Eurasian SAT change and the related circulation systems change in projections.

In this study, we used averaging over a relatively short period, namely 30 years, compared to the longer period, such as 100 years, which can largely remove the internal variability (Dai & Bloecker, 2019; Huang et al., 2020). We investigated the model uncertainty among the CMIP6 models of simulating the future climatology of the SAT changes over the Eurasian continent and the associated changes in the large-scale circulations. The rest of the paper is organized as follows. Section 2 introduces data, definitions of circulation indices and methods. The results are presented in Section 3, including the intermodel deviations of the SAT changes and the circulations changes, the leading intermodel spread of the simulated SAT changes, and the physical linkage with the large-scale circulations changes, which could be traced to the sea surface temperature (SST) conditions. The summary and discussion are provided in Section 4.

2. Data and Method

2.1. Data

We used the monthly outputs of historical runs and the SSP2-4.5 runs from 24 recently released CMIP6 models (Eyring et al., 2016), which include SAT, sea-level pressure (SLP), 850 and 200 hPa meridional and zonal winds, 500 hPa geopotential height, 200 hPa geopotential height, vertical velocity, and SST. We used all the ensemble members available and calculated the ensemble mean for each model, full of the relevant atmospheric and oceanic variables, for historical and projected data at the end of the 21st century. The basic information of the models is summarized in Table 1. All the model data were interpolated onto a $1 \times 1^{\circ}$ grid (90°S – 90°N , 0° – 357.5°E) before analysis. The multimodel mean (MMM) is the arithmetic ensemble mean of the 24 model simulations. This study focused on the climatology mean changes in the boreal winter (December–January–February), which are the 2071–2100 mean minus the 1979–2014 mean. We used the global mean of SAT change to represent the change under global warming. The future changes investigated in our study were normalized by the global mean of winter SAT change in each model (hereafter short for changes), removing the effect of the intermodel uncertainty from the climate sensitivity in each model (Huang et al., 2020; Zhou et al., 2020).

Table 1
List of the 24 CMIP6 Models Used in This Study

Model number	Model name	Modeling center and country	Atmospheric; oceanic resolution (lon × lat: number of grids, L: Vertical levels)	Number of members
1	ACCESS-CM2	Commonwealth Scientific and Industrial Research Organization and Bureau of Meteorology, Australia	192 × 144/L85; 360 × 300/L50	4
2	ACCESS-ESM1-5		192 × 145/L38; 360 × 300/L50	40
3	BCC-CSM2-MR	Beijing Climate Center, China Meteorological Administration, China	320 × 160/L46; 360 × 232/L40	1
4	CESM2-WACCM	National Center for Atmospheric Research, USA	288 × 192/L70; 320 × 384/L60	1
5	CMCC-CM2-SR5	Fondazione Centro Euro-Mediterraneo sui Cambiamenti Climatici, Italy	288 × 192/L30; 362 × 292/L50	1
6	CMCC-ESM2		288 × 192/L30; 362 × 292/L50	1
7	EC-Earth3		512 × 256/L91; 362 × 292/L75	1
8	EC-Earth3-CC	AEMET, Spain; BSC, Spain; CNR-ISAC, Italy; DMI, Denmark; ENEA, Italy; FMI, Finland; Geomar, Germany; ICHEC, Ireland; ICTP, Italy; IDL, Portugal; IMAU, The Netherlands; IPMA, Portugal; KIT, Karlsruhe, Germany; KNMI, The Netherlands; Lund University, Sweden; Met Eireann, Ireland; NLeSC, The Netherlands; NTNU, Norway; Oxford University, UK; surfSARA, The Netherlands; SMHI, Sweden; Stockholm University, Sweden; Unite ASTR, Belgium; University College Dublin, Ireland; University of Bergen, Norway; University of Copenhagen, Denmark; University of Helsinki, Finland; University of Santiago de Compostela, Spain; Uppsala University, Sweden; Utrecht University, The Netherlands; Vrije Universiteit Amsterdam, The Netherlands; Wageningen University, The Netherlands	512 × 256/L91; 362 × 292/L75	3
9	EC-Earth3-Veg		512 × 256/L91; 362 × 292/L75	1
10	EC-Earth3-Veg-LR		320 × 160/L62; 362 × 292/L75	1
11	FGOALS-f3-L	Chinese Academy of Sciences, China	360 × 180/L32; 360 × 218/L30	1
12	FGOALS-g3		180 × 90/L26; 360 × 218/L30	1
13	FIO-ESM-2-0	FIO (First Institute of Oceanography, China), QNLM (Qingdao National Laboratory for Marine Science and Technology, China)	192 × 288/L26; 320 × 384/L60	3
14	GFDL-ESM4	National Oceanic and Atmospheric Administration, Geophysical Fluid Dynamics Laboratory, USA	360 × 180/L49; 720 × 576/L75	3
15	INM-CM4-8	Institute for Numerical Mathematics, Russia	180 × 120/L21; 360 × 318/L40	1
16	INM-CM5-0		180 × 120/L73; 720 × 720/L40	1
17	IPSL-CM6A-LR	Institut Pierre Simon Laplace, France	144 × 143/L79; 362 × 332/L75	2
18	KIOST-ESM	Korea Institute of Ocean Science and Technology, Republic of Korea	192 × 96/L32; 360 × 200/L52	1
19	MIROC6	JAMSTEC (Japan Agency for Marine-Earth Science and Technology, Japan), AORI (Atmosphere and Ocean Research Institute, Japan), NIES (National Institute for Environmental Studies, Japan), and R-CCS (RIKEN Center for Computational Science, Japan)	256 × 128/L81; 360 × 256/L63	50
20	MRI-ESM2-0	Meteorological Research Institute, Japan	320 × 160/L80; 320 × 160/L61	1
21	NESM3	Nanjing University of Information Science and Technology, China	192 × 96/L47; 384 × 362/L46	1
22	NorESM2-LM	NorESM Climate modeling Consortium consisting of CICERO (Center for International Climate and Environmental Research, Oslo 0349), MET-Norway (Norwegian Meteorological Institute, Oslo 0313), NERSC (Nansen Environmental and Remote Sensing Center, Bergen 5006), NILU (Norwegian Institute for Air Research, Kjeller 2027), UiB (University of Bergen, Bergen 5007), UiO (University of Oslo, Oslo 0313) and UNI (Uni Research, Bergen 5008), Norway. Mailing address: NCC, c/o MET-Norway, Henrik Mohns plass 1, Oslo 0313, Norway	144 × 96/L32; 360 × 384/L70	1
23	NorESM2-MM		288 × 192/L32; 360 × 384/L70	1
24	TaiESM1	Research Center for Environmental Changes, Academia Sinica, Taiwan, China	288 × 192/L30; 320 × 384/L60	1

2.2. Definitions of Circulation Indices

To measure the changes in the large-scale circulations, five indices were chosen in this study. The negative value of the regional average of the changes in SLP (45°–55°N, 60°–120°E) and the positive value of the regional average (30°–60°N, 160°–180°W) to identify the strength of negative SLP anomalies over Eurasia (hereafter short for Low), and positive SLP anomalies over North Pacific (hereafter short for High), respectively.

The change in the intensity of the western subtropical jet (hereafter short for WSJ) is defined as the average changes in a 5°-wide 200-hPa zonal wind band centered on the western subtropical jet axis, which is characterized by maximum zonal winds over the active region of the western subtropical jet (15°–35°N, 45°–90°E). Following previous studies (Lu, 2004; Yan et al., 2019; Zhou et al., 2020), the changes in the meridional location of the eastern polar front jet (hereafter short for EPJ) are defined as the difference between the averaged changes of zonal wind at 200-hPa of the band (15°-wide zonal band) on the north side of the polar front jet axis (zonally) over 90°–140°E minus that on the south side. A positive EPJ indicates a northward-shifted eastern polar front jet. The specified regions of each model to calculate the indices vary because of the different locations of the polar front jet axis in each model.

The center of the East Asian trough axis is the minimum point of the 500-hPa eddy height over the region (20°–80°N, 90°E–150°W) (Leung & Zhou, 2015). The eddy height is the deviation of height from the zonal mean. The difference in the changes of 500-hPa eddy height between the northeast of the trough (29°–44°N, 145°E–165°W) and the southwest of the trough (10°–20°N, 105°–155°E) (hereafter short for EAT), represents the changes in the tilt of the trough. The positive value of the EAT indicates the tilt from a quiet northeast-southwest-oriented axis to the north-south-oriented one (Wang et al., 2009).

2.3. Methods

The intermodel standard deviations are used to show the overall discrepancy of the changes in Eurasian SAT and large-scale circulations among the models (Xu & K. Fan, 2022). To analyze the intermodel uncertainty across models, following the previous study (Huang et al., 2022; Zhou et al., 2020), the intermodel Empirical Orthogonal Function (EOF) was performed to extract the intermodel spread of the Eurasian continent SAT change (10°–50°N, 50°–140°E). The first mode in the intermodel EOF analysis was selected as the leading intermodel spread. The composite analysis is also used based on the normalized first principal component (PC1). We separated the models into two groups based on PC1 and used a *t* test to determine whether the differences between the two groups were significant.

Organizational research methods have received a lot of attention because they are the most obvious and current effort to convey the relative contribution of the importance indices (Dunn et al., 1995; Hobson & Gibson, 1983; Johnson & LeBreton, 2004). One of the common methods is the relative weight analysis (RWA) first proposed by Johnson (2000) and developed by Abdella et al. (2021), who integrates linear mixed-effect models (Avilés, 2001) with RWA. In RWA, the original indicators are regressed on the orthogonal variables rather than the orthogonal variables being regressed on the original predictors, avoiding the issue of correlated predictors (Johnson & LeBreton, 2004).

To calculate the relative contributions of different circulation variables defined above, RWA is applied among PC1 and the five circulation indices, addressing the problem of correlated predictors (Johnson, 2000). First, we created a new set of uncorrelated predictors (Z_k), which have the greatest correlation with the orthogonal counterparts of all original drivers (X_j , as Low, High, EAT, WSJ, and EPJ defined in definitions of circulation indices):

$$X_j = \sum a_{jk} Z_k + \varphi \quad (1)$$

where a_{jk} denotes the regression coefficients of X_j on Z_k ; φ represents a disturbance term.

Second, the dependent variable Y (PC1) is regressed on Z_k and the standardized regression coefficients (b_k) are get:

$$Y = \sum b_k Z_k + \chi \quad (2)$$

where χ denotes a disturbance term.

The relative contribution weight of the X_j to Y would be calculated as:

$$\omega_j = \sum a_{jk}^2 b_k^2 \quad (3)$$

3. Results

3.1. The Intermodel Spreads of the Projected Changes in the Winter SAT Over the Eurasian Continent and Associated Large-Scale Circulation Systems

Figure 1 shows the intermodel standard deviations of the changes in the Eurasian continent winter SAT, SLP, the 500-hPa eddy geopotential height field, and 200-hPa zonal wind from the CMIP6 models are shown in Figure 1. The intermodel standard deviations of Eurasian SAT simulations are high over the Tibetan plateau (Figure 1a). The large model deviations of SLP appear in the mid-to-high latitudes, especially over the Icelandic Low, Greenland, the Arctic Ocean, the Tibetan plateau, and the Aleutian Low (Figure 1b), which resemble that of the 500-hPa eddy geopotential height field (Figure 1c), characterized by the large deviations over mid-to-high latitudes at lower and upper levels. The large model deviations of 200-hPa zonal wind mainly exist over the active regions of the jets, especially over the oceanic branch of the subtropical jet (Figure 1d). As reviewed in Section 1, the variations of the large-scale circulations are closely related to the winter SAT over the Eurasian continent. Therefore, we consider the question that whether the large model deviations of atmospheric circulations change can physically explain the uncertainties of the SAT change.

To explore the intermodel uncertainties in each model, the intermodel EOF analysis is applied to investigate the leading intermodel spread of the winter SAT change over the Eurasian continent from the 24 CMIP6 models. The variance fraction of the first EOF mode is 34.2%. The dominant spatial distribution (Figure 2a) shows a uniform warming pattern in Eurasia, except for the slight cooling in Indian Peninsula. The differences among models in Figure 2b indicate the intermodel uncertainties.

To further understand the differences among models associated with the leading intermodel spread, the composite analysis is applied for the positive group (seven models) and the negative group (eight models), based on the criterion of the PC1 exceeding +0.5 and below -0.5, respectively. The SAT change differences between the two groups and the MMM are shown in Figures 3a and 3b. In the positive group (Figure 3a), the warm changes are over the Eurasian continent while the SAT changes are almost opposite in the negative group (Figure 3b). This pattern is particularly evident in the difference between the composite SAT changes in the positive group and those in the negative group (Figure 3c), which resembles the leading intermodel spread in Figure 2a.

Similarly, to understand the relationship between the leading intermodel spread and the change of large-scale atmospheric circulations, we have calculated the difference between the positive and negative groups of the changes in SLP and the 850-hPa winds (Figure 4). The weakened Siberian High and Aleutian Low trigger the evident abnormal cyclone over the mid-to-high latitudes over Eurasia and anticyclone over North Pacific (Figure 4), which weaken the cold air intrusion and thus contribute to the warming over Eurasia (Figure 3c). It is noteworthy that there is a wide belt of 850-hPa winds stretching from the North Atlantic to East Asia, resembling the wave train mentioned in the previous study (Ye et al., 2015).

The leading intermodel spread is also influenced by the differences in the changes of the two groups in the mid-and-upper-level circulations (Figure 5). On the one hand, the 500-hPa eddy geopotential height field exhibits a north-south seesaw pattern in the midlatitudes of the North Pacific and the southeast of Eurasia, indicating the tilt of the East Asian trough (Figure 5a), almost north-south-oriented (Wang et al., 2009). This pattern also resembles the combination of Figures 2b and 2c in Leung and Zhou (2015), which inferred a strong relationship with the weakened Aleutian low and subtropical jet and intensified polar jet, preventing the cold air southward. Accompanied by the tilting trough, this weakened meridional gradient of geopotential height over the mid-to-high latitudes may decelerate the westerlies (Wang et al., 2009).

On the other hand, the significant anomalies in the 500-hPa (Figure 5a) and 200-hPa (Figure 5b) eddy geopotential height reveal a similar pattern, showing the weakened westerlies south of 45°N (Figure 5c). In the upper level, there is an anticyclone over the tropical North Atlantic, an anticyclone over western Europe, a cyclone over west Siberia, and an anticyclone over the western North Pacific in Figure 5b, resembling the wave train induced by the warming over the tropical Atlantic (Ye et al., 2015). It corresponds to the weakened subtropical jet (15°–35°N, 45°–90°E) and northward polar jet (45°–60°N, 90°–140°E) shown in Figure 5c.

The relationship between the changes in the jets and the leading intermodel spread has been linked by the vertical motions, which is shown in Figure 6. Focused on the western entrance of the subtropical jet (45°–90°E), the reduced divergence is found in the south sides of the jet entrance (~30°N) (Figure 6a). Meanwhile, there is

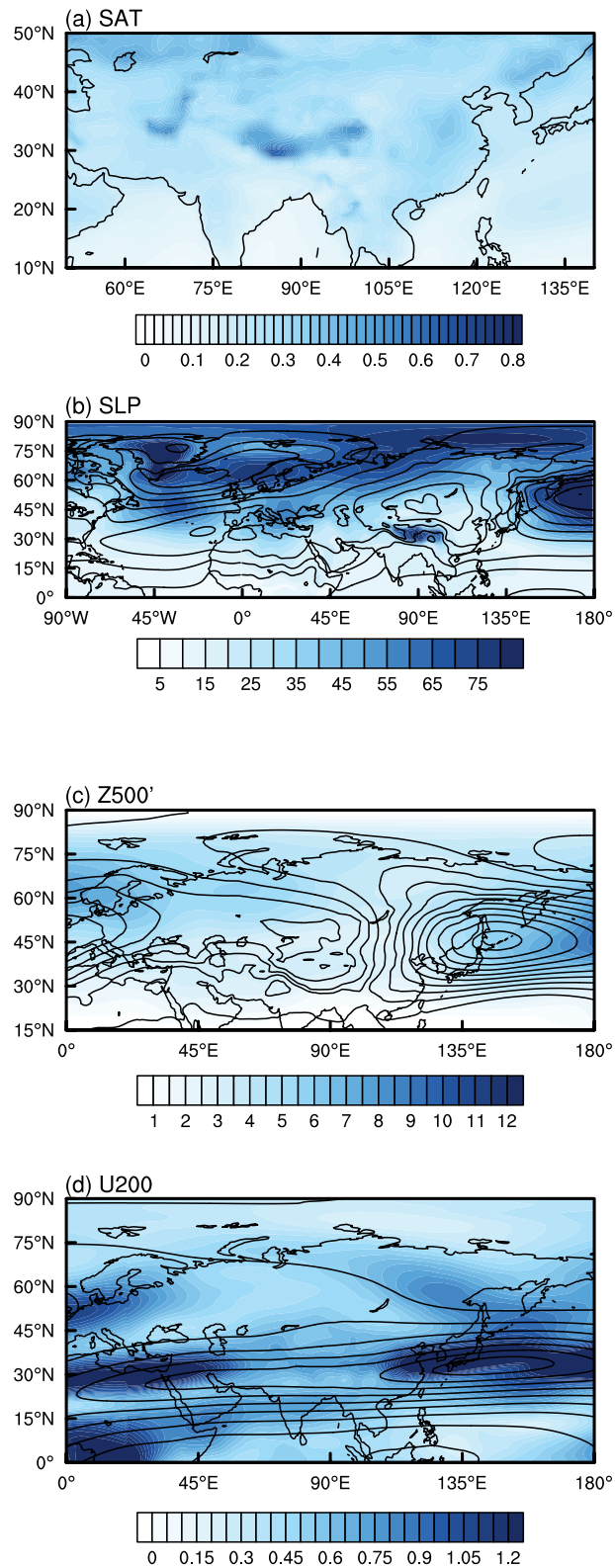


Figure 1. Intermodel standard deviations (shading) of normalized changes in winter surface air temperature (SAT) (a; unit: $K \cdot K^{-1}$), sea-level pressure (SLP) (b; unit: $Pa \cdot K^{-1}$), the 500-hPa eddy geopotential height field (c; unit: $m \cdot K^{-1}$), and 200-hPa zonal wind (d; unit: $m \cdot s^{-1} \cdot K^{-1}$). The contours in (b, c, and d) represent historical multimodel mean (MMM) SLP (b; unit: Pa), the 500-hPa eddy geopotential height (c; unit: m), and 200-hPa zonal wind (d; unit: $m \cdot s^{-1}$).

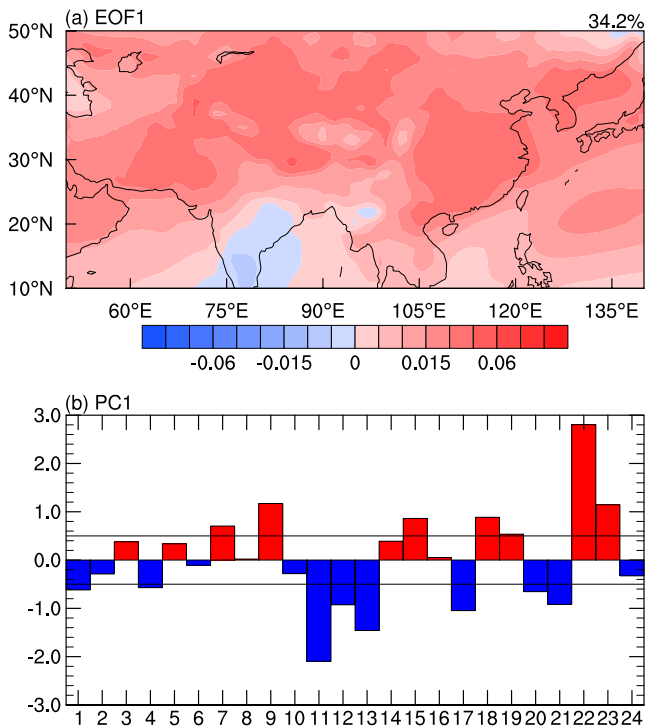


Figure 2. The spatial pattern of the leading intermodel EOF mode of the normalized winter surface air temperature (SAT) change over the Eurasian continent from Coupled Model Intercomparison Project 6 (CMIP6) models (a; unit: $K \cdot K^{-1}$) and the corresponding normalized principal component (b; PC1). The numbers in the x-label in (b) are the model numbers shown in Table 1. The two solid lines in (b) indicate the 0.5 and -0.5 standard deviations. The positive group includes EC-Earth3, EC-Earth3-Veg, INM-CM4-8, KIOST-ESM, MIROC6, NorESM2-LM, and NorESM2-MM (PC1 exceeding $+0.5$) and the negative group includes ACCESS-CM2, CESM2-WACCM, FGOALS-f3-L, FGOALS-g3, FIO-ESM-2-0, IPSL-CM6A-LR, MRI-ESM2-0, and NESM3 (PC1 below -0.5).

a positive anomaly on the north side of the eastern polar jet (90° – 130° E), indicating the eastern polar front jet axis moving northwards (Figure 6b). There is also subsidence in the tropical Atlantic (Figure 6c), corresponding to the anticyclone in Figure 4. The above upper-level circulation field changes anomaly corresponds to the surface winds changes and warm anomaly in the Eurasian continent (Figure 4), via the enhanced upward movement in Eurasia (Huang et al., 2017).

In all, linked to the leading intermodel spread, five large-scale circulations have been revealed, as the weakened Siberian High and Aleutian Low at the surface, the tilting East Asian trough at the midlevel, and the weakened western subtropical jet and northward eastern polar jet at the upper level. To identify the relative contribution of the large-scale circulations to the leading intermodel spread, the RWA method and five indices have been used. At the surface, the Low and High are positively correlated with PC1, with a correlation coefficient of 0.43 and 0.58, respectively. The relative contribution weights of the two SLP variables are 12.73% and 20.43%, respectively. For the variables at the mid-to-high levels, the correlation coefficients between EAT, WSJ, EPI, and PC1 are 0.63, 0.55, and 0.50, respectively. The weights of the three variables are 30.24%, 20.96%, and 15.64%, respectively (Figures 7b and 7c). These high correlations have confirmed the linkage between anomalies of the five large-scale changes and the leading intermodel spread. Combined with the analysis above and previous studies (Zhou et al., 2020; Zhou & Wu, 2015), we can speculate that the warming in Eurasia is attributed a lot to the circulation anomalies, resulting in the leading intermodel spread.

The above analysis indicates that the atmospheric circulation change anomalies may play an important role in the warming pattern, displaying a wave train over the North Atlantic and Eurasia and a tilting East Asian trough. In the prior study, we have established the physical linkage between the intermodel variations in SST and those in SAT over Eurasia (Liu et al., 2022). Here, we aim to investigate whether this relationship can be persisted into the projected SST and SAT. Therefore, we further explored the differences in the winter SST change between the two groups shown in Figure 8, indicating warm SST changes anomalies in the tropical North Atlantic and west-

ern North Pacific. On the one hand, the tropical North Atlantic warming would induce a barotropic wave-type pattern over the eastern North Atlantic and Eurasia (Matsumura & Kosaka, 2019; Ye et al., 2015) as the wave train shown in Figures 4 and 5. Particularly, in the upper level, the positive height anomalies over the tropical Atlantic (Figure 5b) lead to the weakening of the subtropical jet (Figure 5c), thereby contributing to the warming over the Eurasian continent.

On the other hand, the warming over the North Pacific is associated with the enhanced northern and reduced southern meridional temperature gradient over east Asia-North Pacific sector (Sun et al., 2016), via the thermal wind theory, and therefore induces the anomalous positive barotropic height anomalies over there (Sun et al., 2016; Wang et al., 2009), including the anticyclone over the midlatitude region from the coast of East Asia to the North Pacific (Figure 4), the tilt of the East Asian trough, weakened subtropical jet and northward polar jet (Figure 5). These barotropic anomalies in circulation contribute to the warming pattern over the Eurasian continent. Thus, the warming spread over the tropical North Atlantic and North Pacific would affect the spreads in the large-scale circulations and therefore results in the warming spread over the Eurasian continent.

4. Conclusion and Discussions

In this study, we analyzed the intermodel uncertainties of the changes in the winter SAT over Eurasia, along with its relationship with the circulation anomalies of changes in SLP, the East Asian trough, and jets, using the outputs from 24 CMIP6 models. The leading intermodel spread of the winter SAT change over Eurasia is a

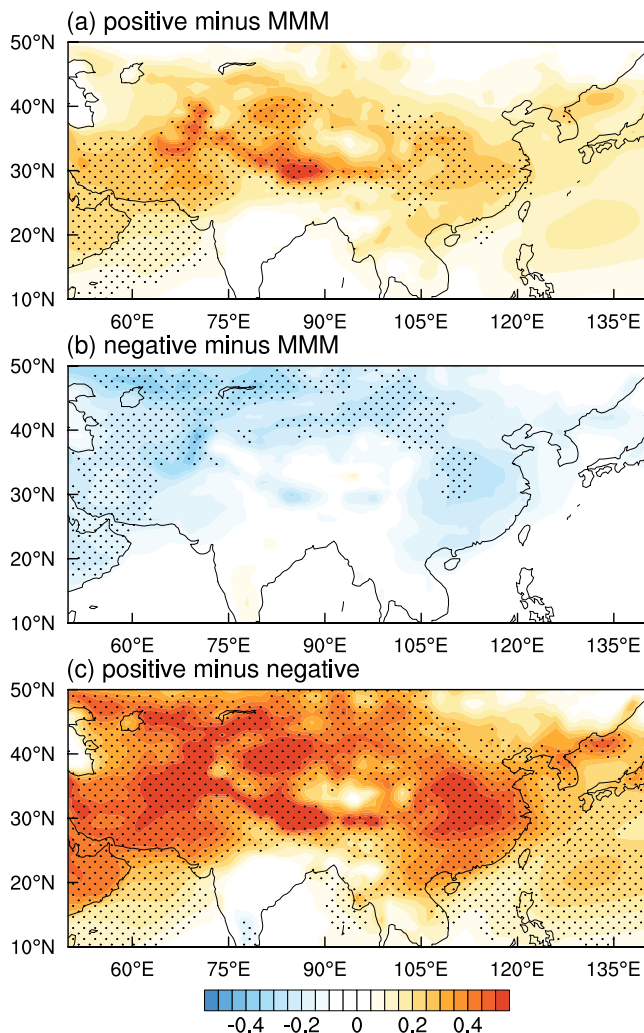


Figure 3. The difference in the composite normalized surface air temperature (SAT) change between the positive group and the multimodel mean (MMM) (a), the negative group and MMM (b), and between the positive group and the negative group (c) (unit: $K \cdot K^{-1}$). Stippling denotes the difference are significant at the 95% confidence level.

warming pattern. We have classified the positive and negative groups based on the criterion of the PC1 exceeding $+0.5$ and below -0.5 and focused on the difference between the two groups, due to the symmetry of the SAT and circulation changes in the two groups. The leading intermodel spread is closely associated with the changes in reduced SLP over mid-to-high latitudes, the enhanced SLP in the western North Pacific and the coast of East Asia, the tilting East Asian trough, along a north-south-oriented, the weakened western subtropical jet and the northward shift of the eastern polar front jet.

The physical linkages among them have been concluded in Figure 9. It shows that the warming is attributed to the negative and positive SLP anomalies that trigger the temperature advection, with weights of 12.73% and 20.43%, respectively. As well, the tilt of the East Asian trough suppresses the southward invasion of cold air, with a weight of 30.24%. The weakened western subtropical jet and the northward eastern polar jet also contribute to the leading pattern through the configuration via the vertical movement, with weights of 20.96% and 15.64%, respectively.

It is speculated that the anomalies of SST changes over the tropical Atlantic and the western North Pacific could affect the projected winter SAT over Eurasia via the large-scale circulations. The warming over the tropical Atlantic could induce a barotropic wave-type pattern over the eastern North Atlantic and Eurasia, including the weakened subtropical jet, ultimately influencing the warming pattern over the Eurasian continent. The warming over the western North Pacific could alter the meridional temperature gradient, giving rise to barotropic positive height anomalies. These height anomalies, comprising the anticyclone over the midlatitude region from the coast of East Asia to the North Pacific, the tilt of the East Asian trough, the weakened subtropical jet and the northward polar jet, contribute to the Eurasian warming. The relationship among the changes in SST, large-scale circulations and SAT have also been summarized in the schematic diagram (Figure 9). Thus, our study has inferred that there is a strong relation between the large-scale circulation changes and SAT changes among models which might be traced to such SST changes.

It is noteworthy that the SST anomaly over the Pacific and the corresponding barotropic anomalies are also consistent with our previous study in historical

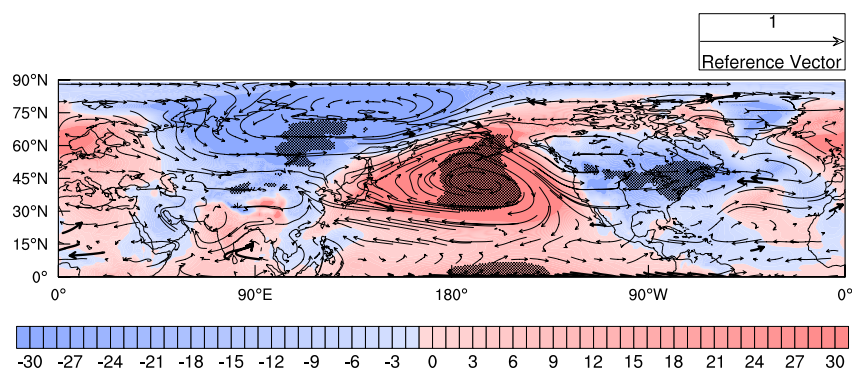


Figure 4. Same as Figure 3c, but for the winter sea-level pressure (SLP) (shaded) (unit: $Pa \cdot K^{-1}$) over the Eurasian continent and the 850-hPa winds (vector) (unit: $m \cdot s^{-1} \cdot K^{-1}$). Stippling denotes the SLP change difference is significant at the 95% confidence level. The medium bolded arrows represent 850-hPa winds difference is significant at the 90% confidence level, while the boldest is significant at the 95% confidence level.

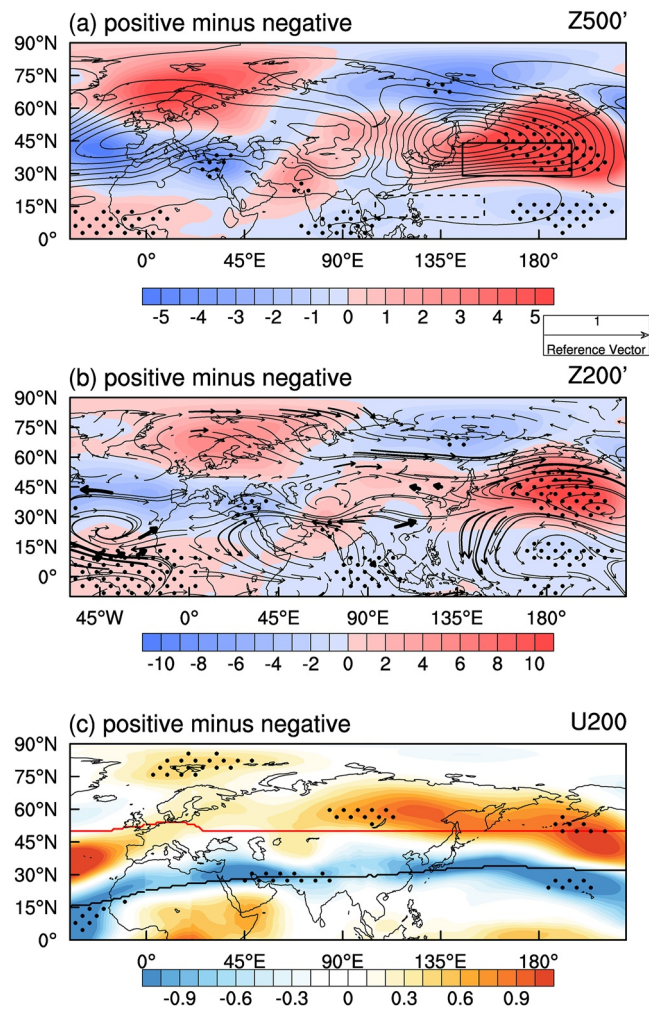


Figure 5. Same as Figure 3, but for the 500-hPa eddy geopotential height field (a) (unit: $\text{m} \cdot \text{K}^{-1}$), the 200-hPa eddy geopotential height field (b) (unit: $\text{m} \cdot \text{K}^{-1}$) and 200-hPa zonal wind (c) (unit: $\text{m} \cdot \text{s}^{-1} \cdot \text{K}^{-1}$). Contour lines in (a) represent the historical MMM of the 500-hPa eddy geopotential height (unit: m). The medium bolded arrows in (b) represent 200-hPa winds (unit: $\text{m} \cdot \text{s}^{-1} \cdot \text{K}^{-1}$) difference is significant at the 90% confidence level, while the boldest is significant at the 95% confidence level. The solid red line and black line in (c) are the polar front jet axis and subtropical jet axis, respectively. Stippling denotes that the 500-hPa eddy geopotential height (a), 200-hPa eddy geopotential height (b), and 200-hPa zonal wind (c) normalized change differences are significant at the 95% confidence level. EAT is calculated as the difference between the black solid (29° – 44°N , 145°E – 165°W) and the dashed boxes (10° – 20°N , 105° – 155°E), representing changes in the tilt of the trough (a).

model uncertainty (Liu et al., 2022). It is suggested that the SST variations and the corresponding barotropic anomalies over the western North Pacific may persist from the historical run to the warmer future, resulting in the intermodel spread of the projected SAT over the Eurasian continent. The long-lived warming is suggested to be related to the anticyclone over the western North Pacific, as a member of the barotropic anomalies, transporting the heat from the tropic (Rivière, 2010), as well as the increased radiation and downward sensible heat flux under greenhouse gas forcing, potentially serving as a bridge to link the external forcing and trough (Miao et al., 2018). In the future work, we will thoroughly investigate the positive feedback mechanism between Pacific warming and positive barotropic anomalies in the warming future, in turn, impact the projected Eurasian SAT. Based on the understanding of this relationship, the uncertainties of projected Eurasian SAT can be constrained.

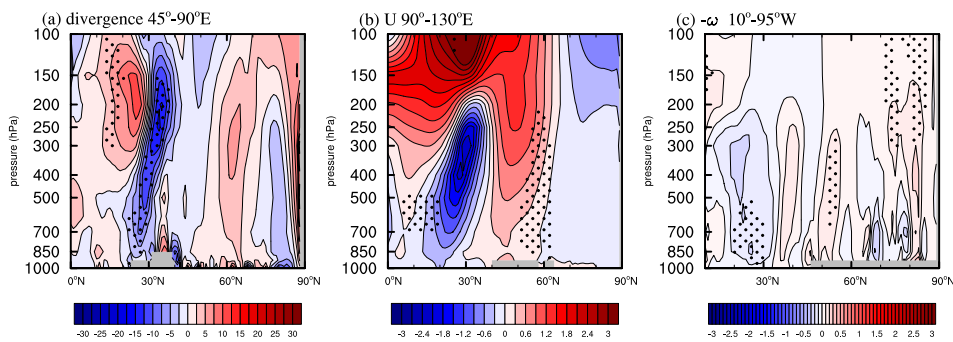


Figure 6. The difference in the composite winter normalized changes of the meridional-height cross section of wind velocity divergence (a, unit: $10^{-7} \text{ s}^{-1} \cdot \text{K}^{-1}$) (45°–90°E), zonal wind (b, unit: $\text{m} \cdot \text{s}^{-1} \cdot \text{K}^{-1}$) (90°–130°E), and vertical velocity (10°–95°W) between the positive and negative groups. Stippling denotes the differences are significant at the 95% confidence level. The gray shade denotes the terrains.

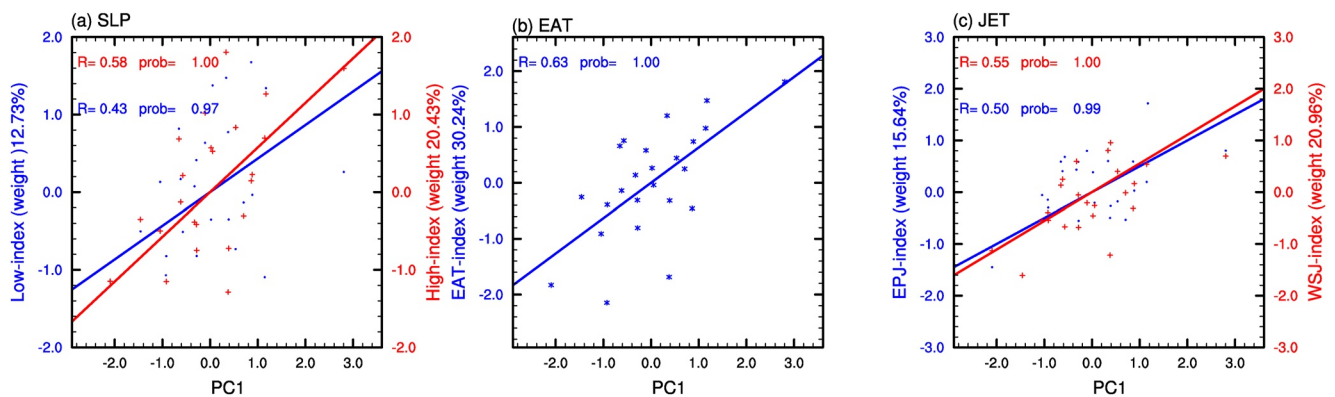


Figure 7. The scatter plots of the normalized principal component (PC1) and five indices of the EAWM among the 25 Coupled Model Intercomparison Project 6 (CMIP6) models: (a) Low (blue) and High (red); (b) EAT (blue); (c) WSJ (red); and EPJ (blue). The five indices have been normalized by their intermodel standard deviations. The correlation coefficients are shown as R and the significant levels are shown as prob. The relative contribution weights are shown along the labels of the Y axis.

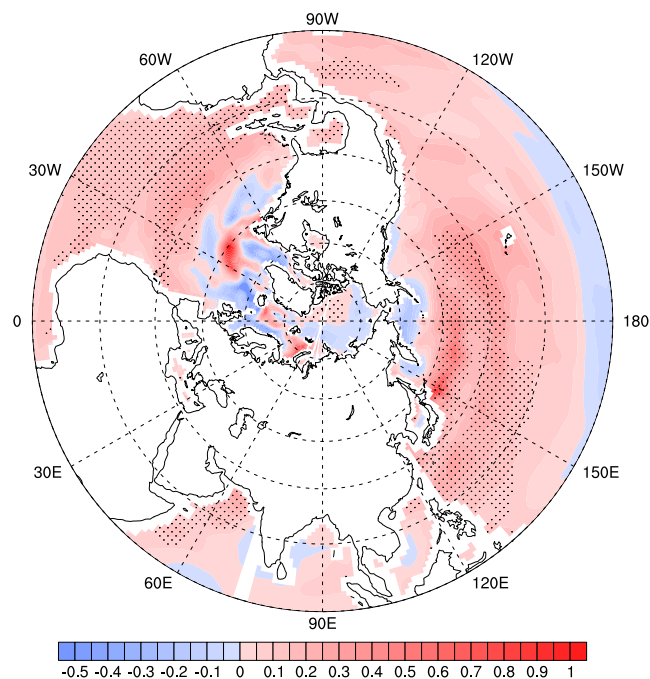


Figure 8. The difference in the composite winter normalized sea surface temperature (SST) changes between the positive and negative group (unit: $\text{K} \cdot \text{K}^{-1}$). Stippling denotes the difference is significant at the 95% confidence level.

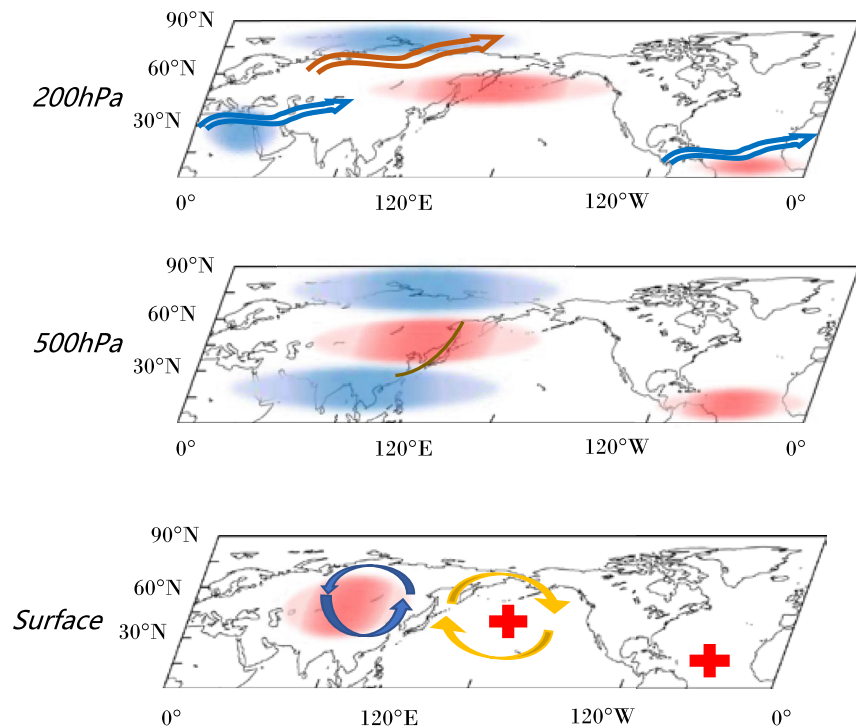


Figure 9. Schematic diagram of the physical linkage among the leading intermodel spread, normalized circulation changes at different levels and normalized sea surface temperature (SST) changes among models. At the surface, the red circle represents warm Eurasia; the yellow and blue curved arrows indicate anticyclone and cyclone circulations, respectively; the red plus sign represents positive SST changes. At 500 hPa, the brown curve indicates the East Asian trough, the red circle represents the positive height changes, and the blue circle represents the negative height changes. At 200 hPa, the orange hollow arrow indicates the northward polar front jet and the blue hollow arrow indicates the weakened subtropical jet while the red circle represents the positive height changes and the blue circle represents the negative height changes.

Data Availability Statement

The CMIP6 model data used in this study can be accessed at the ESGF portal (<https://esgf-node.llnl.gov/projects/esgf-llnl/>) as mentioned in the citation reference (Eyring et al., 2016) [Dataset]; The ERA5 data sets are available at <https://www.ecmwf.int/en/forecasts/datasets/reanalysis-datasets/era5>) as mentioned in the citation reference (Hersbach et al., 2020) [Dataset]. The figures in this manuscript are prepared using NCL software (URL: <https://www.ncl.ucar.edu/>) [software].

Acknowledgments

This study is jointly sponsored by the National Key Research and Development Program of China (Grant 2020YFA0608901), the National Natural Science Foundation of China (Grants 41930969 and 42075020), and the Jiangsu Collaborative Innovation Center for Climate Change.

References

- Abdella, G. M., Kucukvar, M., Ismail, R., Abdelsalam, A. G., Onat, N. C., & Dawoud, O. (2021). A mixed model-based Johnson's relative weights for eco-efficiency assessment: The case for global food consumption. *Environmental Impact Assessment Review*, 89, 106588. <https://doi.org/10.1016/j.eiar.2021.106588>
- Aru, H., Chen, W., & Chen, S. (2021). Is there any improvement in simulation of the wintertime Western Pacific teleconnection pattern and associated climate anomalies in CMIP6 compared to CMIP5 models? *Journal of Climate*, 34(22), 8841–8861. <https://doi.org/10.1175/JCLI-D-21-0016.1>
- Avilés, A. I. (2001). Linear mixed models for longitudinal data. *Technometrics*, 43(3), 375. <https://doi.org/10.1198/tech.2001.s630>
- Chen, X., & Luo, D. (2019). Winter midlatitude cold anomalies linked to North Atlantic sea ice and SST anomalies: The Pivotal role of the potential vorticity gradient. *Journal of Climate*, 32(13), 3957–3981. <https://doi.org/10.1175/JCLI-D-18-0504.1>
- Chowdary, J., Hu, K., Gangiredla, S., Kosaka, Y., Wang, L., & Kundeti, K. (2019). The Eurasian jet streams as conduits for east Asian monsoon variability. *Current Climate Change Reports*, 5, 1–12. <https://doi.org/10.1007/s40641-019-00134-x>
- Cohen, J., Furtado, J. C., Barlow, M. A., Alexeev, V. A., & Cherry, J. E. (2012). Arctic warming, increasing snow cover and widespread boreal winter cooling. *Environmental Research Letters*, 7(1), 014007. <https://doi.org/10.1088/1748-9326/7/1/014007>
- Cohen, J., Screen, J. A., Furtado, J. C., Barlow, M., Whittleston, D., Coumou, D., et al. (2014). Recent Arctic amplification and extreme mid-latitude weather. *Nature Geoscience*, 7(9), 627–637. <https://doi.org/10.1038/ngeo2234>
- Dai, A., & Bloecker, C. E. (2019). Impacts of internal variability on temperature and precipitation trends in large ensemble simulations by two climate models. *Climate Dynamics*, 52(1), 289–306. <https://doi.org/10.1007/s00382-018-4132-4>

- Dunn, W. S., Mount, M. K., Barrick, M. R., & Ones, D. S. (1995). Relative importance of personality and general mental ability in managers' judgments of applicant qualifications. *Journal of Applied Psychology*, *80*(4), 500–509. <https://doi.org/10.1037/0021-9010.80.4.500>
- Eyring, V., Bony, S., Meehl, G. A., Senior, C. A., Stevens, B., Stouffer, R. J., & Taylor, K. E. (2016). Overview of the Coupled Model Intercomparison Project Phase 6 (CMIP6) experimental design and organization [Dataset]. *Geoscientific Model Development*, *9*(5), 1937–1958. <https://doi.org/10.5194/gmd-9-1937-2016>
- Eyring, V., Cox, P. M., Flato, G. M., Gleckler, P. J., Abramowitz, G., Caldwell, P., et al. (2019). Taking climate model evaluation to the next level. *Nature Climate Change*, *9*(2), 102–110. <https://doi.org/10.1038/s41558-018-0355-y>
- Fan, X., Duan, Q., Shen, C., Wu, Y., & Xing, C. (2020). Global surface air temperatures in CMIP6: Historical performance and future changes. *Environmental Research Letters*, *15*(10), 104056. <https://doi.org/10.1088/1748-9326/abb051>
- Gong, H. A., Wang, L., Chen, W., Wu, R. G., Wei, K., & Cui, X. F. (2014). The climatology and interannual variability of the East Asian winter monsoon in CMIP5 models. *Journal of Climate*, *27*(4), 1659–1678. <https://doi.org/10.1175/JCLI-D-13-00039.1>
- Ha, K.-J., Heo, K.-Y., Lee, S.-S., Yun, K.-S., & Jhun, J.-G. (2012). Variability in the East Asian monsoon: A review. *Meteorological Applications*, *19*(2), 200–215. <https://doi.org/10.1002/met.1320>
- Han, S., & Sun, J. (2018). Impacts of autumnal Eurasian snow cover on predominant modes of boreal winter surface air temperature over Eurasia. *Journal of Geophysical Research: Atmospheres*, *123*, 10076–101091. <https://doi.org/10.1029/2018JD028443>
- Hersbach, H., Bell, B., Berrisford, P., Hirahara, S., Horányi, A., Muñoz-Sabater, J., et al. (2020). The ERA5 global reanalysis [Dataset]. *Quarterly Journal of the Royal Meteorological Society*, *146*(730), 1999–2049. <https://doi.org/10.1002/qj.3803>
- Hobson, C. J., & Gibson, F. W. (1983). Policy capturing as an approach to understanding and improving performance appraisal: A review of the literature. *Academy of Management Review*, *8*(4), 640–649. <https://doi.org/10.2307/258265>
- Honda, M., Inoue, J., & Yamane, S. (2009). Influence of low arctic sea-ice minima on anomalously cold Eurasian winters. *Geophysical Research Letters*, *36*, L08707. <https://doi.org/10.1029/2008GL037079>
- Huang, D., Dai, A., Yang, B., Yan, P., Zhu, J., & Zhang, Y. (2019). Contributions of different combinations of the IPO and AMO to recent changes in winter east Asian jets. *Journal of Climate*, *32*(5), 1607–1626. <https://doi.org/10.1175/JCLI-D-18-0218.1>
- Huang, D., Dai, A., & Zhu, J. (2020). Are the transient and equilibrium climate change patterns similar in response to increased CO₂? *Journal of Climate*, *33*(18), 8003–8023. <https://doi.org/10.1175/JCLI-D-19-0749.1>
- Huang, D., Dai, A., Zhu, J., Zhang, Y., & Kuang, X. (2017). Recent winter precipitation changes over eastern China in different warming periods and the associated east Asian jets and oceanic conditions. *Journal of Climate*, *30*(12), 4443–4462. <https://doi.org/10.1175/JCLI-D-16-0517.1>
- Huang, D., Liu, A., Zheng, Y., & Zhu, J. (2022). Inter-model spread of the simulated East Asian summer monsoon rainfall and the associated atmospheric circulations from the CMIP6 models. *Journal of Geophysical Research: Atmospheres*, *127*, e2022JD037371. <https://doi.org/10.1029/2022JD037371>
- Inoue, J., Hori, M. E., & Takaya, K. (2012). The role of Barents Sea ice in the wintertime cyclone track and emergence of a warm-arctic cold-Siberian anomaly. *Journal of Climate*, *25*(7), 2561–2568. <https://doi.org/10.1175/JCLI-D-11-00449.1>
- Jiang, D. B., Hu, D., Tian, Z. P., & Lang, X. M. (2020). Differences between CMIP6 and CMIP5 models in simulating climate over China and the East Asian monsoon. *Advances in Atmospheric Sciences*, *37*(10), 1102–1118. <https://doi.org/10.1007/s00376-020-2034-y>
- Johnson, J. W. (2000). A heuristic method for estimating the relative weight of predictor variables in multiple regression. *Multivariate Behavioral Research*, *35*(1), 1–19. https://doi.org/10.1207/s15327906mbr3501_1
- Johnson, J. W., & LeBreton, J. M. (2004). History and use of relative importance indices in organizational research. *Organizational Research Methods*, *7*(3), 238–257. <https://doi.org/10.1177/1094428104266510>
- Leung, M. Y.-T., & Zhou, W. (2015). Variation of circulation and East Asian climate associated with anomalous strength and displacement of the East Asian trough. *Climate Dynamics*, *45*(9), 2713–2732. <https://doi.org/10.1007/s00382-015-2504-6>
- Liao, Z., & Zhang, Y. (2013). Concurrent variation between the East Asian subtropical jet and polar front jet during persistent snowstorm period in 2008 winter over southern China. *Journal of Geophysical Research: Atmospheres*, *118*, 6360–6373. <https://doi.org/10.1002/jgrd.50558>
- Liu, A., Huang, Y., & Huang, D. (2022). Inter-model spread of the simulated winter surface air temperature over the Eurasian continent and the physical linkage to the jet streams from the CMIP6 models. *Journal of Geophysical Research: Atmospheres*, *127*, e2022JD037172. <https://doi.org/10.1029/2022JD037172>
- Lu, C., Zhou, B., & Ding, Y. (2016). Decadal variation of the northern hemisphere annular mode and its influence on the East Asian trough. *Journal of Meteorological Research*, *30*(4), 584–597. <https://doi.org/10.1007/s13351-016-5105-3>
- Lu, R. (2004). Associations among the components of the East Asian summer monsoon system in the meridional direction. *Journal of the Meteorological Society of Japan Series II*, *82*(1), 155–165. <https://doi.org/10.2151/jmsj.82.155>
- Luo, B. H., Luo, D. H., Dai, A. G., Simmonds, I., & Wu, L. X. (2021). A connection of winter Eurasian cold anomaly to the modulation of Ural blocking by ENSO. *Geophysical Research Letters*, *48*, e2021GL094304. <https://doi.org/10.1029/2021GL094304>
- Luo, B. H., Wu, L. X., Luo, D. H., Dai, A. G., & Simmonds, I. (2019). The winter midlatitude-arctic interaction: Effects of North Atlantic SST and high-latitude blocking on arctic sea ice and Eurasian cooling. *Climate Dynamics*, *52*(5–6), 2981–3004. <https://doi.org/10.1007/s00382-018-4301-5>
- Luo, D., Xiao, Y., Yao, Y., Dai, A., Simmonds, I., & Franzke, C. L. E. (2016). Impact of Ural blocking on winter warm arctic-cold Eurasian anomalies. Part I: Blocking-induced amplification. *Journal of Climate*, *29*(11), 3925–3947. <https://doi.org/10.1175/JCLI-D-15-0611.1>
- Luo, D. H., Xiao, Y. Q., Diao, Y. N., Dai, A. G., Franzke, C. L. E., & Simmonds, I. (2016). Impact of Ural blocking on winter warm arctic-cold Eurasian anomalies. Part II: The link to the North Atlantic oscillation. *Journal of Climate*, *29*(11), 3949–3971. <https://doi.org/10.1175/JCLI-D-15-0612.1>
- Luo, X., & Wang, B. (2017). How predictable is the winter extremely cold days over temperate East Asia? *Climate Dynamics*, *48*(7–8), 2557–2568. <https://doi.org/10.1007/s00382-016-3222-4>
- Luo, X., & Zhang, Y. (2015). The linkage between upper-level jet streams over East Asia and east Asian winter monsoon variability. *Journal of Climate*, *28*(22), 9013–9028. <https://doi.org/10.1175/JCLI-D-15-0160.1>
- Matsumura, S., & Kosaka, Y. (2019). Arctic–Eurasian climate linkage induced by tropical ocean variability. *Nature Communications*, *10*(1), 3441. <https://doi.org/10.1038/s41467-019-11359-7>
- McCusker, K. E., Fyfe, J. C., & Sigmund, M. (2016). Twenty-five winters of unexpected Eurasian cooling unlikely due to Arctic sea-ice loss. *Nature Geoscience*, *9*(11), 838–842. <https://doi.org/10.1038/ngeo2820>
- Miao, J., Wang, T., Wang, H., Zhu, Y., & Sun, J. (2018). Interdecadal weakening of the East Asian winter monsoon in the mid-1980s: The roles of external forcings. *Journal of Climate*, *31*(21), 8985–9000. <https://doi.org/10.1175/JCLI-D-17-0868.1>
- Monerie, P.-A., Wainwright, C. M., Sidibe, M., & Akinsanola, A. A. (2020). Model uncertainties in climate change impacts on Sahel precipitation in ensembles of CMIP5 and CMIP6 simulations. *Climate Dynamics*, *55*(5), 1385–1401. <https://doi.org/10.1007/s00382-020-05332-0>

- Mori, M., Watanabe, M., Shiogama, H., Inoue, J., & Kimoto, M. (2014). Robust Arctic sea-ice influence on the frequent Eurasian cold winters in past decades. *Nature Geoscience*, 7(12), 869–873. <https://doi.org/10.1038/ngeo2277>
- Moss, R. H., Edmonds, J. A., Hibbard, K. A., Manning, M. R., Rose, S. K., van Vuuren, D. P., et al. (2010). The next generation of scenarios for climate change research and assessment. *Nature*, 463(7282), 747–756. <https://doi.org/10.1038/nature08823>
- Nakamura, H., Miyasaka, T., Kosaka, Y., Takaya, K., & Honda, M. (2010). Northern hemisphere extratropical tropospheric planetary waves and their low-frequency variability: Their vertical structure and interaction with transient eddies and surface thermal contrasts. In D.-Z. Sun, & F. Bryan (Eds.) *Climate dynamics: Why does climate vary?* (pp. 149–179). AGU. <https://doi.org/10.1029/2008GM000789>
- Overland, J., Wood, K. R., & Wang, M. (2011). Warm Arctic-cold continents: Climate impacts of the newly open arctic sea. *Polar Research*, 30(1), 15787. <https://doi.org/10.3402/polar.v30i0.15787>
- Rama, H. O., Roberts, D., Tignor, M., Poloczanska, E. S., Mintenbeck, K., Alegria, A., et al. (2022). Climate change 2022: Impacts, Adaptation and Vulnerability. In *Contribution of working group I to the sixth assessment report of the intergovernmental panel on climate change*. IPCC. <https://doi.org/10.1017/9781009325844>
- Rivière, G. (2010). Role of Rossby wave breaking in the west Pacific teleconnection. *Geophysical Research Letters*, 37, L11802. <https://doi.org/10.1029/2010GL043309>
- Solomon, S. C., Qin, D., Manning, M. R., Chen, Z. R., Marquis, M., Averyt, K. B., et al. (2007). Climate change 2007: The physical science basis. In *Contribution of working group I to the fourth assessment report of the intergovernmental panel on climate change. Summary for Policymakers*. IPCC.
- Sun, J., Wu, S., & Ao, J. (2016). Role of the North Pacific sea surface temperature in the East Asian winter monsoon decadal variability. *Climate Dynamics*, 46(11), 3793–3805. <https://doi.org/10.1007/s00382-015-2805-9>
- Takaya, K., & Nakamura, H. (2005a). Geographical dependence of upper-level blocking formation associated with intraseasonal amplification of the Siberian high. *Journal of the Atmospheric Sciences*, 62(12), 4441–4449. <https://doi.org/10.1175/JAS3628.1>
- Takaya, K., & Nakamura, H. (2005b). Mechanisms of intraseasonal amplification of the cold Siberian high. *Journal of the Atmospheric Sciences*, 62(12), 4423–4440. <https://doi.org/10.1175/JAS3629.1>
- Wang, L., Chen, W., Zhou, W., & Huang, R. (2009). Interannual variations of East Asian trough Axis at 500 hPa and its association with the East Asian winter monsoon pathway. *Journal of Climate*, 22(3), 600–614. <https://doi.org/10.1175/2008JCLI2295.1>
- Wang, L., Qian, Y., Leung, L. R., Chen, X., Sarangi, C., Lu, J., et al. (2021). Multiple metrics informed projections of future precipitation in China. *Geophysical Research Letters*, 48, e2021GL093810. <https://doi.org/10.1029/2021GL093810>
- Wu, W., Ji, F., Hu, S., He, Y., Wei, Y., Xu, Z., & Yu, H. (2022). Future evolution of global land surface air temperature trend based on Coupled Model Intercomparison Project Phase 6 models. *International Journal of Climatology*, 42(15), 7611–7627. <https://doi.org/10.1002/joc.7668>
- Xu, M., Xu, H., & Ma, J. (2016). Responses of the East Asian winter monsoon to global warming in CMIP5 models. *International Journal of Climatology*, 36(5), 2139–2155. <https://doi.org/10.1002/joc.4480>
- Xu, Z., & Fan, K. (2022a). Inter-model spreading of changes in East Asian winter monsoon circulation under 1.5 and 2.0°C global warming targets. *International Journal of Climatology*, 42(8), 4360–4378. <https://doi.org/10.1002/joc.7471>
- Xu, Z. Q., & Fan, K. (2022b). Inter-model spreading of changes in East Asian winter monsoon circulation under 1.5 and 2.0 degrees C global warming targets. *International Journal of Climatology*, 42(8), 4360–4378. <https://doi.org/10.1002/joc.7471>
- Yan, Y., Li, C., & Lu, R. (2019). Meridional displacement of the East Asian upper-tropospheric westerly jet and its relationship with the East Asian summer rainfall in CMIP5 simulations. *Advances in Atmospheric Sciences*, 36(11), 1203–1216. <https://doi.org/10.1007/s00376-019-9066-1>
- Yang, S., Lau, K. M., & Kim, K. M. (2002). Variations of the East Asian jet stream and Asian-Pacific-American winter climate anomalies. *Journal of Climate*, 15(3), 306–325. [https://doi.org/10.1175/1520-0442\(2002\)015<0306:VOTEAJ>2.0.CO;2](https://doi.org/10.1175/1520-0442(2002)015<0306:VOTEAJ>2.0.CO;2)
- Yao, S. L., Luo, J. J., & Huang, G. (2016). Internal variability-generated uncertainty in east Asian climate projections estimated with 40 CCSM3 ensembles. *PLoS One*, 11(3), e0149968. <https://doi.org/10.1371/journal.pone.0149968>
- Yao, Y., Luo, D. H., Dai, A. G., & Simmonds, I. (2017). Increased quasi stationarity and persistence of winter Ural blocking and Eurasian extreme cold events in response to arctic warming. Part I: Insights from observational analyses. *Journal of Climate*, 30(10), 3549–3568. <https://doi.org/10.1175/jcli-d-16-0261.1>
- Ye, K., Wu, R., & Liu, Y. (2015). Interdecadal change of Eurasian snow, surface temperature, and atmospheric circulation in the late 1980s. *Journal of Geophysical Research: Atmospheres*, 120, 2738–2753. <https://doi.org/10.1002/2015JD023148>
- Zhang, L., Fraedrich, K., Zhu, X., Sielmann, F., & Zhi, X. (2015). Interannual variability of winter precipitation in Southeast China. *Theoretical and Applied Climatology*, 119(1), 229–238. <https://doi.org/10.1007/s00704-014-1111-5>
- Zhang, Y., Sperber, K. R., & Boyle, J. S. (1997). Climatology and Interannual variation of the East Asian winter monsoon: Results from the 1979–95 NCEP/NCAR reanalysis. *Monthly Weather Review*, 125(10), 2605–2619. [https://doi.org/10.1175/1520-0493\(1997\)125<2605:CAIVOT>2.0.CO;2](https://doi.org/10.1175/1520-0493(1997)125<2605:CAIVOT>2.0.CO;2)
- Zhang, Y., & Xiao, C. (2013). Variability modes of the winter upper-level wind field over Asian mid- high latitude region. *Atmospheric and Oceanic Science Letters*, 6(5), 295–299. <https://doi.org/10.1080/16742834.2013.11447097>
- Zhang, Y., Yan, P., Liao, Z., Huang, D., & Zhang, Y. (2019). The winter concurrent meridional shift of the East Asian jet streams and the associated thermal conditions. *Journal of Climate*, 32(7), 2075–2088. <https://doi.org/10.1175/JCLI-D-18-0085.1>
- Zhang, Y. C., Wang, D. Q., & Ren, X. J. (2008). Seasonal variation of the meridional wind in temperate jet stream and its relationship to the Asian monsoon. *Acta Meteorologica Sinica*, 22(4), 446–454.
- Zhou, L.-T., & Wu, R. (2015). Interdecadal variability of winter precipitation in Northwest China and its association with the North Atlantic SST change. *International Journal of Climatology*, 35(6), 1172–1179. <https://doi.org/10.1002/joc.4047>
- Zhou, S., Huang, G., & Huang, P. (2020). Inter-model spread of the changes in the East Asian summer monsoon system in CMIP5/6 models. *Journal of Geophysical Research: Atmospheres*, 125, 2020JD033016. <https://doi.org/10.1029/2020JD033016>